Biometals (2011) 24:759–768
DOI 10.1007/s10534-011-9422-9

The role of phosphate on Omniscan® dechelation: an in vitro relaxivity study at pH 7

Robic Caroline · Catoen Sarah · Goltstein De Marie-Christine · Idée Jean-Marc · Port Marc

Received: 27 July 2010 / Accepted: 8 February 2011 / Published online: 10 March 2011

Abstract Nephrogenic systemic fibrosis (NSF), a disease occurring in patients with severe renal failure, may be linked to injections of gadolinium chelates, contrast agents used for magnetic resonance imaging. A hypothesis frequently proposed to explain NSF is dissociation of Gd^{3+} from its chelate, possibly from a deep storage compartment. Numerous in vivo and in vitro studies have been performed in an attempt to determine the extent of this dechelation and to understand its mechanism. Proton-assisted dechelation and transmetallation are the most widely described mechanisms of dechelation. This study investigated the possible ligand exchange role played by phosphate in the dechelation mechanism. Omniscan® dechelation was monitored in vitro by relaxivity measurements performed at physiological pH with different concentrations of phosphate buffer and in the presence of endogenous cations. Dechelation experiments performed on phosphate buffer alone showed that phosphate may induce gadolinium release by ligand exchange when the phosphate concentration in the buffer is higher than 130 mM for an Omniscan® concentration of 1.25 mM. This corresponds to a Gd/phosphate ratio of 10^{-2}. This ratio could be reached in vivo, especially in deep compartments such as bone. The presence of endogenous cations (Zn^{2+}, Cu^{2+} or Ca^{2+}) has also been demonstrated to accelerate the kinetics of gadolinium release, either by catalysing ligand exchange or by inducing a transmetallation mechanism. The Omniscan® formulation was also tested and the added Ca–DTPA–BMA was shown to increase dechelation kinetics in these experiments. This striking result may question the value of the Omniscan® formulation in the context of NSF.

Keywords Gadolinium chelate · Omniscan® · Dechelation · Transmetallation · Relaxivity · NSF

R. Caroline (✉) · C. Sarah · G. De Marie-Christine · I. Jean-Marc · P. Marc
Guerbet, Research Division, BP 57400, 95943 Roissy CdG Cedex, France
e-mail: caroline.robic@guerbet-group.com

Introduction

Nephrogenic systemic fibrosis (NSF) is a rare but highly disabling disease occurring in patients with severe or end-stage renal failure (Cowper et al. 2000). The association between NSF and gadolinium chelates, contrast agents used for magnetic resonance imaging, was suggested in 2006 by two European teams (Grobner 2006; Marckmann et al. 2006). The most extensively described of the numerous hypotheses proposed to explain this disease is that NSF is due to dissociation of Gd^{3+} from its chelate (Idee et al. 2008; Morcos 2007; Perazella 2007), possibly from a "deep storage compartment" which has been

proposed to be bone tissue (Thakral et al. 2007). It has been speculated that the risk of dissociation is enhanced in the presence of renal failure resulting in increased circulation time of Gd chelates in the body, subsequently triggering fibrosis (Morcos 2007; Perazzella 2007). This hypothesis has led to a renewed interest in the physicochemical properties of Gd chelates, especially their stability. Many papers have described the thermodynamic and kinetic properties of Gd chelates (Idee et al. 2006; Port et al. 2008). Thermodynamic and kinetic properties are well described physicochemically, but they are much more difficult to assess in vivo.

In the present study, in vitro relaxivity measurements were performed at physiological pH, at different phosphate buffer concentrations and in the presence of endogenous cations. These experiments were based on the method described by Laurent et al. (2001, 2006) which allows quantitative evaluation of Gd^{3+} release from its chelate in the presence of endogenous cations at pH 7. The experiments were performed in phosphate buffer with an equimolar ratio of Gd chelate and endogenous cation. Dechelation induces the formation of a $GdPO_4$ precipitate with a negligible influence on relaxivity (Laurent et al. 2001; Port et al. 2008). A decrease of the relaxation rate ratio $R_1^p(t)/R_1^p(t=0)$ as a function of time would therefore reflect formation of the $GdPO_4$ precipitate and the magnitude of this decrease would quantify the amount of precipitate formed. The aim of this study was to demonstrate the role of phosphate in these experiments and to highlight the role of ligand exchange in the dechelation mechanism. The role of endogenous cations via transmetallation mechanism has been well described in the literature (Idee et al. 2006; Port et al. 2008), but this study was designed to investigate whether phosphate, used as buffer, plays a role in the dechelation phenomenon.

This study was performed with formulated (i.e. Omniscan®, see Fig. 1) and nonformulated Gd–DTPA–BMA, as this compound exhibits poor kinetic stability and the highest degree of dechelation (Port et al. 2008). Although pharmaco-epidemiologic data are obviously difficult to interpret, it has been reported that the vast majority of published cases of NSF were associated with Gd–DTPA–BMA, Omniscan® (Broome 2008; Cowper 2007; Kanal et al. 2007; Thomsen 2006).

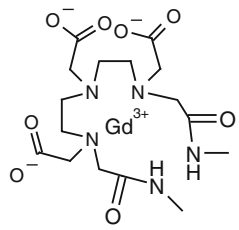

Fig. 1 Gd–DTPA–BMA structure. Omniscan® is Gd–DTPA–BMA formulated with Ca–DTPA–BMA (Na^+ salt) 5% (25 mmol/l)

Materials and methods

Chemicals

Phosphate buffer was prepared from KH_2PO_4 and Na_2HPO_4, purchased from Prolabo. 335 mM phosphate buffer ($[KH_2PO_4] = 0.13$ mol/l, $[Na_2HPO_4] = 0.205$ mol/l) was used in all experiments. In one experiment, the phosphate concentration varied from 500 to 67 mmol/l. All buffers had a pH of 7.

$ZnCl_2$ was purchased from Merck, $CaCl_2$ was purchased from Calbiochem and $CuCl_2$ was purchased from Janssen. The added cation concentration was always 1.25 mM in the final solution except in one experiment in which the Zn^{2+} concentration varied from 0.25 to 6.25 mM. In the case of added Ca^{2+} in formulated and unformulated Gd–DTPA–BMA (Fig. 5), the Ca^{2+} in the formulation was not taken into account.

Commercial Omniscan® was purchased from GE Healthcare SA (Vélizy-Villacoublay, France) and nonformulated Gd–DTPA–BMA was synthesised in our laboratory. A concentration of 1.25 mM was used in all experiments in order to perform relaxivity measurements.

Sample preparation

Two solutions were prepared extemporaneously. The first solution contained 2.5 mM Omniscan® or Gd–DTPA–BMA in phosphate buffer. The second solution contained the endogenous cation in the same phosphate buffer or phosphate buffer only for experiments with no endogenous cations. These two solutions were mixed and a first measurement of water proton relaxation rates (R_1) was performed immediately to give the $t = 0$ point.

Analytic instrumentation

Water proton paramagnetic longitudinal relaxation rates (R_1^p) were measured at 37°C and 0.47 T on a Bruker Minispec Relaxometer PC-20.

330 µl of supernatant were introduced into glass vials (40 × 8.2 mm) with caps, and these tubes were then placed in 10-mm diameter tubes and kept at 37°C in a waterbath between measurements.

Fitting

Curve fitting was performed according to the best result obtained with a monoexponential curve:

$$\frac{R_1^p}{R_1^p(t=0)} = \exp(-kt)$$

or a biexponential curve:

$$\frac{R_1^p}{R_1^p(t=0)} = A + \frac{1-A}{2}(\exp(-k_1 t) + \exp(-k_2 t))$$

Results

Figure 2 represents the ratio of the relaxation rate at time t over the relaxation rate at $t = 0$ (R_1^p (t)/R_1^p ($t = 0$)) as a function of time for a 1.25 mM Omniscan® solution in phosphate buffer. As explained in the introduction, the only relaxing molecule in this experiment is Gd–DTPA–BMA. Indeed if dechelation occurs, Gd precipitates with phosphate and GdPO4 has no relaxation effect. It results from this that R_1^p is directly proportional to Gd–DTPA–BMA concentration (R_1^p = [Gd–DTPA–BMA] * $r_{1\text{Gd–DTPA–BMA}}$). And so we have:

$$\frac{R_1^p(t)}{R_1^p(t=0)} = \frac{[\text{Gd}-\text{DTPA}-\text{BMA}](t)}{[\text{Gd}-\text{DTPA}-\text{BMA}](t=0)}$$

The relaxation rate decreased with time for a phosphate buffer concentration higher than 130 mM. Solid lines represent a monoexponential fit and dotted lines represent a biexponential fit. The kinetic constant values are shown in Table 1: k represents the kinetic constant for a monoexponential fit and k_1 and k_2 the kinetic constants for the biexponential fit. The value of A in the biexponential formula is 0 and 0.16 for phosphate concentrations of 500 and 335 mM, respectively. The inset in Fig. 2 represents the kinetic constant of the monoexponential fit (k) as a function of phosphate concentration: the relation was found to be linear.

The same relaxivity measurements were performed with an equimolar (1.25 mM) solution of Omniscan® and Zn^{2+} in pure water (pH = 7) instead of phosphate buffer. No change of relaxivity was detected over 2 days (data not shown).

However, in experiments conducted in phosphate buffer, Zn^{2+} was shown to play an important role in the dechelation mechanism. Figure 3 represents R_1^p (t)/R_1^p ($t = 0$) as a function of time for 1.25 mM Omniscan® in 335 mM phosphate buffer without Zn^{2+} and with various concentrations of Zn^{2+}. The presence of Zn^{2+} increased the kinetic constant. Two regimes were observed. The first regime corresponds

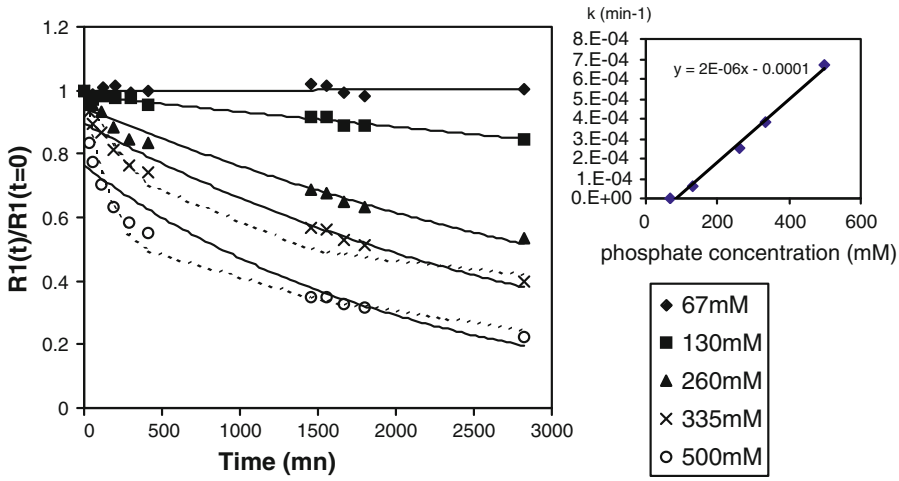

Fig. 2 R_1^p (t)/R_1^p ($t = 0$) as a function of time for 1.25 mM Omniscan® in different concentrations of phosphate buffer. *Solid lines* represent a monoexponential fit and *dotted lines* represent a biexponential fit. The *inset* represents k, the kinetic constant of the monoexponential fit as a function of phosphate concentration

Table 1 k represents the kinetic constant for a monoexponential fit and k_1 and k_2 represent the kinetics constants for a biexponential fit from data from Fig. 2

Phosphate concentration (mM)	k (min^{-1})	k_1 (min^{-1})	k_2 (min^{-1})
67	4×10^{-6}		
130	6×10^{-5}		
260	2.5×10^{-4}		
335	3.8×10^{-4}	2.5×10^{-3}	1.7×10^{-4}
500	6.7×10^{-4}	6×10^{-3}	2.5×10^{-4}

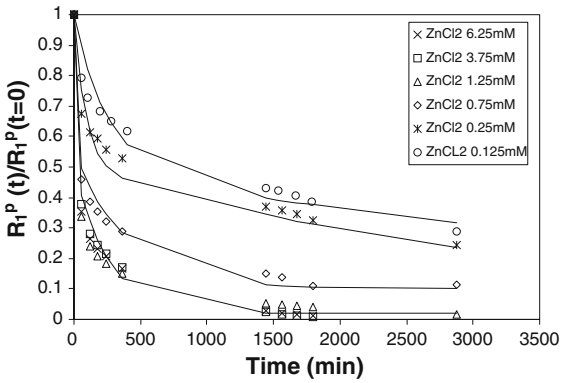

Fig. 3 R_1^p $(t)/R_1^p$ $(t = 0)$ as a function of time for 1.25 mM Omniscan® in 335 mM phosphate buffer with different $ZnCl_2$ concentrations

to low Zn^{2+} concentrations (lower than 0.75 mM). In this regime, the higher the Zn^{2+} concentration, the more rapid was the dechelation phenomenon. The second regime corresponds to higher Zn^{2+} concentrations. In this regime, the kinetics constant is independent of Zn^{2+} concentration. All fits were performed with a biexponential curve and Table 2 shows the fitted parameters: k_1, k_2 and A. Figure 4a and b present k_1 and k_2, respectively, as a function of

Table 2 Kinetic constants (k_1 and k_2) and A from a biexponential fit at different $ZnCl_2$ concentration from data from Fig. 3

[$ZnCl_2$] (mM)	k_1 (min^{-1})	k_2 (min^{-1})	A
0.125	0.004	1.6×10^{-4}	0
0.25	0.013	2.6×10^{-4}	0
0.75	0.07	2.5×10^{-3}	0.07
1.25	0.14	4×10^{-3}	0.02
3.75	0.14	4×10^{-3}	0.02
6.25	0.14	4×10^{-3}	0.02

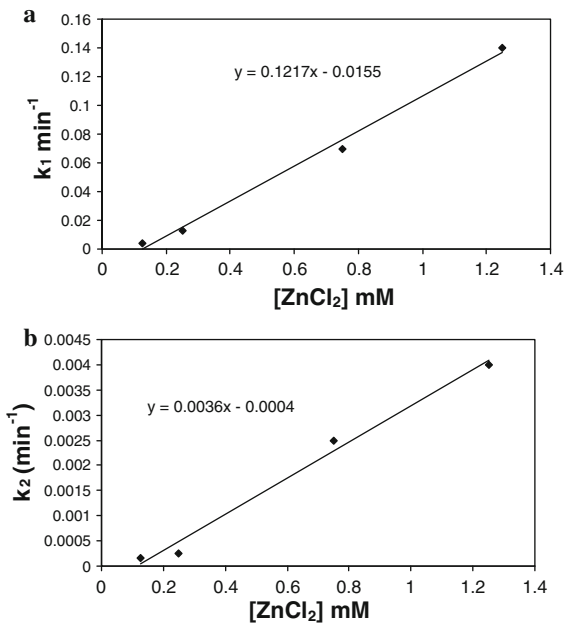

Fig. 4 **a** k_1 as a function of $ZnCl_2$ concentration for 335 mM phosphate buffer. **b** k_2 as a function of $ZnCl_2$ concentration for 335 mM phosphate buffer

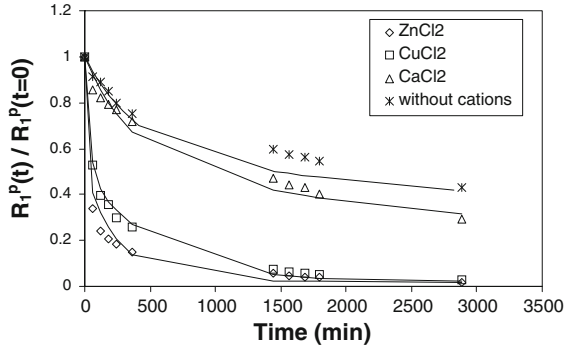

Fig. 5 R_1^p $(t)/R_1^p$ $(t = 0)$ as a function of time for 1.25 mM Omniscan® in 335 mM phosphate buffer with 1.25 mM of various endogenous cations

Table 3 Kinetic constants (k_1 and k_2) and A from a biexponential fit for 1.25 mM of various added cations at 335 mM phosphate buffer from data from Fig. 5

	k_1 (min^{-1})	k_2 (min^{-1})	A
Zn	1.4×10^{-1}	4×10^{-3}	0.02
Cu	3×10^{-2}	1.9×10^{-3}	0.02
Ca	3×10^{-3}	3.5×10^{-4}	0.16
Without cations	2.5×10^{-3}	1.7×10^{-4}	0.16

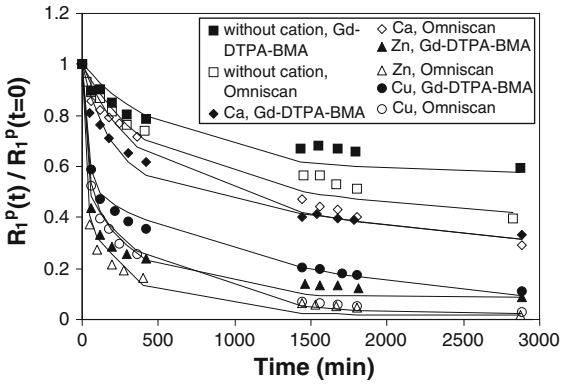

Fig. 6 R_1^p $(t)/R_1^p$ $(t = 0)$ as a function of time for 1.25 mM Omniscan® or Gd–DTPA–BMA in 335 mM phosphate buffer with 1.25 mM of various endogenous cations. *Solid symbols* correspond to nonformulated Gd–DTPA–BMA and *empty symbols* correspond to Omniscan®

Table 4 Omniscan® and Gd–DTPA–BMA kinetic constants (k_1 and k_2) and A from a biexponential fit for 1.25 mM of various added cations at in 335 mM phosphate buffer from data from Fig. 6

		k_1 (min^{-1})	k_2 (min^{-1})	A
Zn	Omniscan®	0.14	4×10^{-3}	0.02
	Gd–DTPA–BMA	0.1	2.8×10^{-3}	0.09
Cu	Omniscan®	3×10^{-2}	1.9×10^{-3}	0.02
	Gd–DTPA–BMA	2.7×10^{-2}	6.7×10^{-4}	0.02
Ca	Omniscan®	3×10^{-3}	3.5×10^{-4}	0.16
	Gd–DTPA–BMA	5.6×10^{-3}	3.5×10^{-4}	0.16
Without cation	Omniscan®	2.5×10^{-3}	1.7×10^{-4}	0.16
	Gd–DTPA–BMA	1.6×10^{-3}	4×10^{-6}	0.16

Zn concentration. A linear relation was observed in both cases.

The effect of two other cations (Ca^{2+} and Cu^{2+}) was also tested. Figure 5 represents R_1^p $(t)/R_1^p$ $(t = 0)$ as a function of time for 1.25 mM Omniscan® in 335 mM phosphate buffer without endogenous cations or with 1.25 mM Zn^{2+}, Cu^{2+} and Ca^{2+}. Cu^{2+} and Zn^{2+} had very similar effects, while Ca^{2+} had a much weaker effect.

Nonformulated Gd–DTPA–BMA was tested according to the same protocol as commercial Omniscan®. Figure 6 compares the results obtained for Omniscan® and Gd–DTPA–BMA in 335 mM phosphate buffer with or without 1.25 mM Zn^{2+}, Ca^{2+}, Cu^{2+}. All fits were performed with a biexponential curve and Table 4 shows the fitted parameters: k_1, k_2 and A. In the presence of phosphate, without added cations, dechelation occurred more rapidly for Omniscan® than in the case of Gd–DTPA–BMA. When Zn^{2+} or Cu^{2+} were added, dechelation still occurred more rapidly with Omniscan® than in the case of Gd–DTPA–BMA. However, Ca^{2+} induce an inversed effect and only on k_1.

Discussion

Under physiological or pathological conditions, the amount of free Gd^{3+} that can be released in the body depends on both the dissociation rate of the Gd chelate (i.e. kinetic stability) and its thermodynamic constant. We have recently stressed (Idee et al. 2006; Port et al. 2008) that, in vivo, high kinetic stability combined with a high thermodynamic constant appear to minimize the amount of free gadolinium released in the body.

Two main mechanisms have been described in the literature to explain gadolinium release from Gd chelates (Port et al. 2008):

- a dechelation mechanism corresponding to the reaction:

$$GdL^n \leftrightarrows Gd^{3+} + L^{n-3} \quad (1)$$

This reaction can actually occur via two mechanisms: spontaneous or proton-assisted dissociation of the Gd^{3+} chelate possibly catalysed by endogenous metals (Sarka et al. 2000).

- or a transmetallation mechanism of the gadolinium chelate by endogenous metals, particularly Ca^{2+}, Cu^{2+} and Zn^{2+}) corresponding to the reaction:

$$GdL^n + M^{2+} \leftrightarrows Gd^{3+} + ML^{n-1} \quad (2)$$

This metal exchange reaction can occur via two mechanisms (Brücher 2002):

– Spontaneous or proton-assisted dissociation of the Gd^{3+} chelate followed by rapid reaction of the free ligand with endogenous metal ions.
– Direct attack of the endogenous ion on the chelate via formation of a dinuclear intermediate GdLM followed by the formation of ML.

Some authors have described the ligand exchange mechanism via the solubility constant of Gd chelates (Cacheris et al. 1990; Lauffer 1987; Merbach and Toth 2001), but did not consider this mechanism to be the main mechanism.

In order to describe the in vivo dissociation of Gd chelates, several in vitro studies have been performed at physiological pH including an endogenous cation such as Fe^{3+}, Cu^{2+}, Zn^{2+} or Ca^{2+} and/or anions that can compete with the ligand such as PO_4^{3-} or CO_3^{2-} (Frenzel et al. 2008; Laurent et al. 2001, 2006; Magerstät et al. 1986; Puttagunta et al. 1996; Sarka et al. 2000, 2002; Tweedle et al. 1991; Tweedle 1992). In all these in vitro experiments performed at physiological pH, linear chelates were characterized by poor kinetic stability, especially nonionic molecules such as Gd–DTPA–BMA. In contrast, macrocyclic chelates were characterized by very high kinetic inertia.

From a more fundamental and mechanistic point of view, the mechanism discussed in these papers is that of transmetallation. However, ligand exchange plays a key role corresponding to the following reaction

$$GdL^n + L_1^{m-3} \leftrightarrows GdL_1^m + L^{n-3} \quad (3)$$

Indeed, the role of endogenous cations has been clearly emphasised in the transmetallation mechanism but the present experiments demonstrate that phosphate plays a major role. As reported by Frenzel et al., the transmetallation constant does not explain the extent of the dechelation phenomenon (Frenzel et al. 2008), possibly because the role of phosphate is usually ignored in Gd dechelation. Phosphate may act in parallel with endogenous cations (Gabricevic et al. 2004), but may also play a major role, which may be amplified or catalysed by endogenous cations.

In the experiment conducted by Laurent et al. (2001, 2006), the initial solution was composed of a Gd chelate and an equimolar concentration of Zn^{2+} in a 67 mM phosphate buffer. It must be stressed that Zn^{2+} precipitates in phosphate buffer with a very high thermodynamic constant:

$$3Zn^{2+} + 2PO_4^{3-} \rightarrow Zn_3(PO_4)_2$$
$$K = \left[Zn^{2+}\right]^3\left[PO_4^{3-}\right]^2 = 10^{-35} \quad (4)$$

Consequently, the concentration of Zn^{2+} in solution is very low in comparison to the initial gadolinium equimolar concentration.

This very low Zn^{2+} concentration highlights the fact that phosphate plays a major role in dechelation.

The main reactions that can occur in solution are as follows:

$$GdL^n \leftrightarrows Gd^{3+} + L^{n-3} \quad \frac{1}{K_{Gd}} = \frac{[Gd^{3+}][L^{n-3}]}{[GdL^n]} \quad (5)$$

$$Zn^{2+} + L^{n-3} \leftrightarrows ZnL^{n-1} \quad K_{Zn} = \frac{[ZnL^{n-1}]}{[Zn^{2+}][L^{n-3}]} \quad (6)$$

$$Gd^{3+} + PO_4^{3-} \rightarrow GdPO_4 \quad K_{GdPO_4} = \left[Gd^{3+}\right]\left[PO_4^{3-}\right] \quad (7)$$

$$3Zn^{2+} + 2PO_4^{3-} \rightarrow Zn_3(PO_4)_2$$
$$K_{Zn_3(PO_4)_2} = \left[Zn^{2+}\right]^3\left[PO_4^{3-}\right]^2 \quad (8)$$

$GdPO_4$ and $Zn_3(PO_4)_2$ are precipitates.

For numerical calculations, apparent thermodynamic constant at pH 7 are used.

The conditional stability constants characterizing Omniscan® at pH 7 are:

$$Gd{-}DTPA{-}BMA \leftrightarrows Gd^{3+} + DTPA{-}BMA^{3-}$$
$$K_{Gd}^{cond} = 10^{14.9}$$

$$Zn{-}DTPA{-}BMA^{-} \leftrightarrows Zn^{2+} + DTPA{-}BMA^{3-} \quad K_{Zn}^{cond} = 10^{10.1}$$

The apparent phosphate solubility constants at pH 7 are calculated as follows:

$$K_{GdPO_4}^{cond} = K_{GdPO_4}\left(1 + \frac{[H^+]^3}{K_{a_1}K_{a_2}K_{a_3}} + \frac{[H^+]^2}{K_{a_2}K_{a_3}} + \frac{[H^+]}{K_{a_3}}\right)$$

where K_{a_1}, K_{a_2} and K_{a_3} are the acidity constants characterizing phosphoric acid.

We find:

$$K_{GdPO_4}^{cond} = 10^{-16.5}$$

$$K_{Zn_3(PO_4)_2}^{cond} = K_{Zn_3(PO_4)_2} \times \left(1 + \frac{[H^+]^3}{K_{a_1}K_{a_2}K_{a_3}} + \frac{[H^+]^2}{K_{a_2}K_{a_3}} + \frac{[H^+]}{K_{a_3}}\right)^2$$

$$K_{Zn_3(PO_4)_2}^{cond} = 10^{-23.4}$$

Ligand exchange is characterized by the reaction:

$$GdL^n + PO_4^{3-} \rightarrow GdPO_4 + L^{n-3} \quad (9)$$

$$K = \frac{[L^{n-3}]}{[GdL^n][PO_4^{3-}]} = \frac{1}{K_{Gd}K_{GdPO_4}} \quad (10)$$

Numerical values, changing thermodynamic constant by conditional thermodynamic constants give:

$$K = 1/\left(10^{14.9}10^{-16.5}\right) = 10^{1.6}$$

and transmetallation is characterized by the reaction:

$$GdL^n + Zn^{2+} \leftrightarrows ZnL^{n-1} + Gd^{3+} \quad (11)$$

$$K = \frac{[ZnL^{n-1}][Gd^{3+}]}{[GdL^n][Zn^{2+}]} = \frac{K_{Zn}}{K_{Gd}} \quad (12)$$

Numerical values, changing thermodynamic constant by conditional thermodynamic constants give:

$$K = 10^{10.1}/10^{14.9} = 10^{-4.8}$$

Comparison of Eq. 5 (dechelation), Eq. 11 (transmetallation) and Eq. 9 (ligand exchange) demonstrates that, from a thermodynamic point of view, the predominant mechanism should be ligand exchange.

Laurent et al. (2001, 2006) did not demonstrate any effect of phosphate on dechelation of a 2.5 mM Omniscan® solution in 67 mM phosphate buffer. We also did not observe any effect of 67 mM phosphate buffer on Omniscan® dechelation. In order to investigate a possible ligand exchange mechanism, experiments were also performed with higher concentrations of phosphate buffer (Fig. 2).

Figure 2 shows that dechelation occurred for a 1.25 mM Omniscan® solution in phosphate buffer concentrations equal to or greater than 130 mM, even without endogenous cations.

The occurring reaction here is:

$$Gd{-}DTPA{-}BMA + PO_4^{3-} \rightarrow GdPO_4 + DTPA{-}BMA^{3-}$$

We have:

$$\frac{d[Gd{-}DTPA{-}BMA]}{dt} = k[Gd{-}DTPA{-}BMA][PO_4^{3-}]$$

As $[PO_4{}^{3-}]$ can be considered as constant in each experiment (greater concentration as compared to others in the sample), this reaction is a pseudo first order one that should be fitted by a monoexponential curve.

A monoexponential model closely fits the experimental data until a phosphate concentration of 260 mM. For 335 and 500 mM phosphate, both monoexponential and biexponential fits are presented. Although neither model gives a close fit, the monoexponential kinetic constant is linear with phosphate concentration (Fig. 2 inset): this would correspond to a pseudo first-order kinetic condition with a kinetic constant k of 2×10^{-6} min^{-1} mM^{-1}.

Furthermore, no change in relaxivity over time was observed in an equimolar solution of Zn^{2+} and Omniscan® in water although an increase in relaxivity with release of Gd^{3+} would have been expected.

These two experiments are in favour of a ligand exchange mechanism and illustrate the key role of phosphate buffer in these in vitro experiments.

The effect of Zn^{2+} combined with that of phosphate on dechelation was tested at different concentrations (Fig. 3). Two regimes were observed. In the first regime (low Zn^{2+} concentrations), the higher the Zn^{2+} concentration, the more rapid was the dechelation phenomenon. In the second regime (high Zn^{2+} concentrations), the kinetic constant was independent of Zn^{2+} concentration. The kinetic-limiting mechanism in this second regime is a reaction that does not involve Zn^{2+}. These results can be interpreted in two different ways: ligand exchange and transmetallation may both occur or Zn^{2+} may catalyse the ligand exchange. Furthermore, the curves showed a better fit with a biexponential model than with a monoexponential model. This characteristic was also reported by Laurent et al. for Omniscan® (2006). This biexponential modelling is generally interpreted by a two-compartment model. One hypothesis to explain this phenomenon would be that zinc interacts with Omniscan® in both its soluble form and its phosphate precipitate form.

In this experiment, phosphate concentrations were obviously high compared to endogenous phosphate concentrations (1–1.2 mM in adults). This high phosphate concentration allowed complete dechelation of Omniscan® in 3 days. NSF may appear several months after gadolinium chelate injections. It has been speculated that gadolinium chelates may be sequestrated into "deep" structures such as bone (Gibby et al. 2004; Thakral et al. 2007; White et al. 2006). Following administration, gadolinium chelates distribute into body "compartments" (defined as a pharmacokinetically distinguishable pool in terms of the drug concentration–time profile). In the case of lanthanide chelates, a three-compartment model, including bone as a "deep" compartment (i.e. a

compartment associated with slow release of the compound) has been proposed by Hirano and Suzuki (1996). Of note, in rats with impaired renal function, lanthanum was observed in the outer edge of mineralized bone (Behets et al. 2005). It can be speculated that the Gd^{3+}/phosphate ratio in bone tissue is of the same order of magnitude as that used in the present experiments. Calcium and phosphorus are present in bone in a 2:1 ratio, predominantly as crystalline structures called hydroxyapatite (70% of bone tissue). Hydroxyapatite includes calcium phosphate, calcium carbonate, calcium fluoride, calcium hydroxide and citrate (Hedges and Van Klinken 1992).

About 125 mmol of body calcium are present in the exchangeable calcium pool, mainly located on the bone-forming surface and representing 0.4–1.0% of total bone calcium. Interestingly, most of this calcium is in the form of rapidly mobilisable salts such as $CaHPO_4$. A daily net of about 27 mmol of phosphorus is absorbed into the exchangeable phosphorus pool. About 29% of this pool is corresponds to the skeletal mineralization front (Hruska et al. 2008). In bone, the composition of interstitial fluid is similar to that of plasma except that the phosphate concentration is higher while calcium, sodium and magnesium concentrations are lower (Aukland 1984). Lastly, osteodystrophy is frequently associated with chronic kidney disease (CKD) (mostly excess bone resorption). Loss of phosphorus homeostasis due to excretion failure results in hyperphosphataemia in CKD patients. The skeleton contributes to this hyperphosphataemia (Hruska et al. 2008). It can be proposed that a pseudo-equilibrium may be reached locally, resulting in gradual release of free Gd^{3+}. Furthermore, we can try to extrapolate these results by using in vivo concentrations of 1 mM phosphate and 20 μM zinc. The apparent kinetic constants at these concentrations (calculated from data of Fig. 4) would be:

$$k_{app1} = 7.3 \times 10^{-6}\,min^{-1}$$

$$k_{app2} = 2.15 \times 10^{-7}\,min^{-1}$$

A 40% decomplexation of Omniscan® would take place in 130 days. Although Omniscan® accumulation in these deep structures is low, a high proportion of the ligand would be decomplexed, according to our model.

The effect of Ca^{2+} and Cu^{2+} was also tested (Fig. 5). The greatest difference between Cu^{2+} and Zn^{2+} concerns the k_1 value that is equal to 0.14 min^{-1} for Zn and 3×10^{-2} min^{-1} for Cu (Table 3). Ca^{2+} had weaker effect at the concentration tested: 1.25 mM. On Fig. 5, the extrapolation at an infinite time reveals the thermodynamic equilibrium. These extrapolations are in accordance with the thermodynamic constant values of DTPA–BMA with Ca^{2+}, Cu^{2+} and Zn^{2+} that are respectively log $K = 7.2$, 13 and 12 at 25°C.

Because of their relatively low stability, pharmaceutical solutions of Gd–DTPA–BMA include a relatively large amount of calcium complexes (25 mmol/l). Such excipients are intended to ensure the absence of free Gd^{3+} cations in pharmaceutical solutions for the duration of their shelf lives. The impact of formulation on dechelation was studied (Fig. 6). The dechelation kinetic in phosphate buffer without cations was more rapid for Omniscan® than for Gd–DTPA–BMA. The kinetic constants of the biexponential fit k_1 and k_2 were higher for Omniscan® than for Gd–DTPA–BMA: $k_1 = 2.5 \times 10^{-3}$ and $k_2 = 1.7 \times 10^{-4}$ min^{-1} for Omniscan® whereas $k_1 = 1.6 \times 10^{-3}$ and $k_2 = 4 \times 10^{-6}$ min^{-1} for Gd–DTPA–BMA (Table 4). Similar results were observed when Zn^{2+} or Cu^{2+} was added: decomplexation of Omniscan® is always more rapid (greater k_1 and k_2 values) than decomplexation of Gd–DTPA–BMA. In the presence of Ca^{2+}, the k_1 value was higher for Gd–DTPA–BMA than for Omniscan® while formulation had no effect on k_2 in the presence of Ca^{2+}.

These striking results may question the value of formulation of Gd chelates in the context of NSF. One explanation for this increased dechelation kinetic with formulated Omniscan® may be catalysis by the calcium chelate.

Frenzel et al. (2008) studied dechelation in human serum of the commercially available Gd chelates by HPLC-ICP-MS analysis with or without an excess of phosphate. They found that dechelation of formulated and nonformulated Gd–DTPA–BMA was the same with a 10 mM excess of phosphate in human serum. In contrast, the initial dissociation kinetic was faster for nonformulated Gd–DTPA–BMA in human serum without an excess of phosphate. The phosphate concentration in our experiments was even higher than in those conducted by Frenzel et al. with an excess of phosphate. This may explain why our experiments showed an increase in the dechelation

kinetic for Omniscan® compared to nonformulated Gd–DTPA–BMA in a large excess of phosphate. In contrast, Sieber et al. (2008) studied the Gd concentration in skin, liver and femur of healthy male rats receiving repeated intravenous injections of Omniscan® and Gd–DTPA–BMA. They found a lower Gd concentration in rat skin with formulated Omniscan® than with Gd–DTPA–BMA but no differences were observed in the femur.

Conclusion

Basically, three different mechanisms can give rise to dissociation between Gd^{3+} and its chelate:

– dechelation corresponding to the reaction:

$$GdL^n \leftrightarrows Gd^{3+} + L^{n-3}$$

This reaction can occur spontaneously or via proton-assisted dissociation.

– transmetallation of Gd^{3+} by an endogenous metal, especially, Zn^{2+}, Cu^{2+}, Ca^{2+}, corresponding to the reaction:

$$GdL^n + M^{2+} \leftrightarrows Gd^{3+} + ML^{n-1}$$

– ligand exchange:

$$GdL^n + L_1^{m-3} \leftrightarrows GdL_1^m + L^{n-3}$$

The present study demonstrates that phosphate could induce gadolinium release by ligand exchange when the phosphate concentration in the buffer is higher than 130 mM for a Gd–DTPA–BMA concentration of 1.25 mM. This corresponds to a Gd/phosphate ratio of 10^{-2}. This ratio could be reached in vivo, especially in deep compartments such as bone.

This type of ligand exchange may therefore be involved in the in vivo dechelation of Gd–DTPA–BMA that has been speculated to play a role in the mechanism of NSF.

This point is supported by the fact that the presence of endogenous cations such as Zn^{2+}, Cu^{2+} or Ca^{2+} accelerated the kinetics of gadolinium release, either by catalysing ligand exchange or by inducing a transmetallation mechanism.

Omniscan® formulation was also shown to increase the dechelation kinetic in our experiments. This striking result may question the value of formulation of gadolinium chelates in the context of NSF.

Studies on other chelates are ongoing.

Acknowledgments The authors would like to thank Drs Sophie Laurent and Luce Vander Elst (Department of General, Organic and Biomedical Chemistry, NMR and Molecular Imaging Laboratory, University of Mons-Hainaut, Belgium) for their helpful discussions.

References

Aukland K (1984) Distribution of body fluids: local mechanisms guarding interstitial fluid volume. Am J Physiol 79:395–400

Behets GJ, Verberckmoes SC, Oste L, Bervoets AR, Salomé M, Cox AG, Denton J, De Broe ME, D'Haese PC (2005) Localization of lanthanum in bone of chronic renal failure rats after oral dosing with lanthanum carbonate. Kidney Int 67:1830–1836

Broome DR (2008) Nephrogenic systemic fibrosis associated with gadolinium based contrast agents: a summary of the medical literature reporting. Eur J Radiol 66(2):230–234

Brücher E (2002) Kinetic stability of gadolinium(III) chelates used as MRI contrast agents. In: Topics in current chemistry, vol 221. Springer-Verlag, Berlin

Cacheris WP, Quay SC, Rocklage SM (1990) The relationship between thermodynamics and the toxicity of gadolinium complexes. Magn Reson Imaging 8(4):467–481

Cowper SE (2007) Nephrogenic systemic fibrosis: a review and exploration of the role of gadolinium. Adv Dermatol 23: 131–154

Cowper SE, Robin HS, Steinberg SM, Su LD, Gupta S, LeBoit PE (2000) Scleromyxoedema-like cutaneous diseases in renal-dialysis patients. Lancet 356:1000–1001

Frenzel T, Lengsfeld P, Schirmer H, Hutter J, Weinmann HJ (2008) Stability of gadolinium-based magnetic resonance imaging contrast agents in human serum at 37°C. Investig Radiol 43(12):817–828

Gabricevic M, Anderson DS, Mietzner TA, Crumbliss AL (2004) Kinetics and mechanism of iron(III) complexation by ferric binding protein: the role of phosphate. Biochemistry 43:5811–5819

Gibby WA, Gibby KA, Gibby WA (2004) Comparison of Gd–DTPA–BMA (Omniscan) versus Gd-HP-DO3A (ProHance) retention in human bone tissue by inductively coupled plasma atomic emission spectroscopy. Investig Radiol 39:138–142

Grobner T (2006) Gadolinium: a specific trigger for the development of nephrogenic fibrosing dermopathy and nephrogenic systemic fibrosis? Nephrol Dial Transplant 21:1104–1108

Hedges REM, Van Klinken GJ (1992) A review of current approaches in the pretreatment of bone for radiocarbon dating by AMS. Radiocarbon 34(3):279–291

Hirano S, Suzuki KT (1996) Exposure, metabolism and toxicity of rare earths and related compounds. Environ Health Perspect 104(Suppl 1):85–95

Hruska KA, Mathew S, Lund R, Qiu P, Pratt R (2008) Hyperphosphatemia of chronic kidney disease. Kidney Int 74:148–157

Idee JM, Port M, Raynal I, Schaefer M, Le Greneur S, Corot C (2006) Clinical and biological consequences of transmetallation induced by contrast agents for magnetic resonance imaging: a review. Fundam Clin Pharmacol 20(6):563–576. Review (2007) Erratum in: Fundam Clin Pharmacol 21(3):335

Idee JM, Port M, Medina C, Lancelot E, Fayoux E, Ballet S, Corot C (2008) Possible involvement of gadolinium chelates in the pathophysiology of nephrogenic systemic fibrosis: a critical review. Toxicology 248:77–88

Kanal E, Barkovich AJ, Bell C, Borgstede JP, Bradley WG Jr, Froelich JW, Gilk T, Gimbel JR, Gosbee J, Kuhni-Kaminski E, Lester JW Jr, Nyenhuis J, Parag Y, Schaefer DJ, Sebek-Scoumis EA, Weinreb J, Zaremba LA, Wilcox P, Lucey L, Sass N (2007) ACR guidance document for safe MR practices. Am J Roentgenol 188:1–27

Lauffer RB (1987) Paramagnetic metal complexes as water proton relaxation agents for NMR Imaging: theory and design. Chem Rev 87:901–927

Laurent S, Vander Elst L, Copoix F, Muller RN (2001) Stability of MRI paramagnetic contrast media. A proton relaxometric protocol for transmetallation assessment. Investig Radiol 36:115–122

Laurent S, Vander Elst L, Muller RN (2006) Comparative study of the physicochemical properties of six clinical low molecular weight gadolinium contrast agents. Contrast Media Mol Imaging 1:128–137

Magerstät M, Gansow OT, Brechiel MW, Colcher D, Baltzer L, Knop RH, Girton ME, Naegle M (1986) GdDOTA: an alternative to GdDTPA as T1, 2 relaxation agent for NMR imaging or spectroscopy. Magn Reson Imaging 3:808–812

Marckmann P, Skov L, Rossen K, Dupont A, Damholt MB, Heaf JG, Thomsen HS (2006) Nephrogenic systemic fibrosis: suspected causative role of gadodiamide used for contrast-enhanced magnetic resonance imaging. J Am Soc Nephrol 17:2359–2362

Merbach AE, Toth E (2001) The chemistry of contrast agents in medical magnetic resonance imaging, Chap. 6: stability and toxicity of contrast agents. Wiley, Chichester

Morcos SK (2007) Nephrogenic systemic fibrosis following the administration of extracellular gadolinium-based contrast agents: is the stability of the contrast agent molecule an important factor in the pathogenesis of this condition? Br J Radiol 80:73–76

Perazella MA (2007) Nephrogenic systemic fibrosis, kidney disease and gadolinium: is there a link? Clin J Am Soc Nephrol 2:200–202

Port M, Idee JM, Medina C, Robic C, Sabatou M, Corot C (2008) Efficiency, thermodynamic and kinetic stability of marketed gadolinium chelates and their possible clinical consequences: a critical review. Biometals 21(4):469–490

Puttagunta NR, Gibby WA, Puttagunta VL (1996) Comparative transmetallation kinetics and thermodynamic stability of gadolinium-DTPA bis-glucosamide and other magnetic resonance imaging contrast media. Investig Radiol 10: 619–624

Sarka L, Burai L, Brücher E (2000) The rates of the exchange reactions between $[Gd(DTPA)]^{2-}$ and the endogenous ions Cu^{2+} and Zn^{2+}: a kinetic model for the prediction of the in vivo stability of $[Gd(DTPA)]^{2-}$. Used as a contrast agent in magnetic resonance imaging. Chem Eur J 6(4): 719–724

Sarka L, Burai L, Kiraly R, Zekany L, Brücher E (2002) Studies on the kinetic stabilities of the Gd(3+) complexes formed with the *N*-mono(methylamide), N′-mono(methylamide) and *N*,″-bis(methylamide) derivatives of diethylenetriamine-*N*,*N*,*N*′,*N*″,*N*″-pentaacetic acid. J Inorg Biochem 25 91(1):320–326

Sieber MA, Pietsch H, Walter J, Haider W, Frenzel T, Weinmann HJ (2008) A preclinical study to investigate the development of nephrogenic systemic fibrosis: a possible role for gadolinium based contrast media. Investig Radiol 43:65–75

Thakral C, Alhariri J, Abraham JL (2007) Long-term retention of gadolinium in tissues from nephrogenic systemic fibrosis patient after multiple gadolinium-enhanced MRI scans: case report and implications. Contrast Media Mol Imaging 2(4):199–205

Thomsen H (2006) Nephrogenic systemic fibrosis: a serious late adverse reaction to gadodiamide. Eur Radiol 16: 2619–2621

Tweedle MF (1992) Physicochemical properties of gadoteridol and other magnetic resonance contrast agents. Investig Radiol 27(Suppl 1):S2–S6

Tweedle MF, Hagan JJ, Kumar K, Mantha S, Chang CA (1991) Reaction of gadolinium chelates with endogenously available ions. Magn Reson Imaging 9:409–415

White GW, Gibby WA, Tweedle MF (2006) Comparison of Gd(DTPA–BMA) (Omniscan) versus Gd(HP-DO3A) (ProHance) relative to gadolinium retention in human bone tissue by inductively coupled mass spectroscopy. Investig Radiol 41:272–278